Available online at www.sciencedirect.com
SCIENCE DIRECT®
Journal of Catalysis 227 (2004) 217–226
JOURNAL OF CATALYSIS
www.elsevier.com/locate/jcat

Promoting and poisoning effects of Na and Cl coadsorption on CO oxidation over MgO-supported Au nanoparticles

Peter Broqvist [a,*], Luis M. Molina [b], Henrik Grönbeck [a], Bjørk Hammer [b]

[a] *Department of Applied Physics and Competence Centre for Catalysis, Chalmers University of Technology, SE-412 96 Göteborg, Sweden*
[b] *iNANO and Department of Physics and Astronomy, University of Aarhus, DK-8000 Aarhus C, Denmark*

Received 3 May 2004; revised 8 July 2004; accepted 9 July 2004

Available online 12 August 2004

Abstract

Density-functional theory has been used to study the CO oxidation reaction at model Au/MgO catalysts modified by either Na (an electron donor) or Cl (an electron acceptor) dopants. In agreement with experimental observations, Cl is found to act as a poison, making both the adsorption of O_2 and the formation of the $CO \cdot O_2$ intermediate complexes that mediate the formation of CO_2 on these model catalysts more difficult. The poisoning effect of Cl has a long-ranged character, reaching at least two Au sites away from the adsorbed Cl atom. On the other hand, Na is found to be a promoter, enhancing both O_2 binding and $CO \cdot O_2$ formation. Its promotive character is, however, local, involving the formation of strong Na–O bonds.

Keywords: Model catalysts; Gold catalysts; Particles; Coadsorption; Nanocrystals; Promoter; Poison; Sodium; Chlorine; Kinetics; Surfaces; Energy; Reaction barrier; CO oxidation; DFT

1. Introduction

While the surfaces of bulk gold are known to be catalytically inactive [1], oxide-supported Au nanoparticles display remarkable catalytic properties for several interesting reactions [2,3], with low-temperature CO oxidation being one of the most extensively studied examples [4–16]. The crucial step in catalytic oxidation is O_2 adsorption, and the inertness of gold bulk surfaces is understood from the poor affinity toward molecular oxygen [17–21]. Much effort has been dedicated to understand the origin of the unusual reactivity of nanosized Au particles. The influence of the supported catalysts' properties such as size, type of support, and method of preparation has been explored. As a result, it is now generally accepted that a small particle-size distribution (< 5 nm) is necessary to obtain active catalysts. Also, sizeable differences between active (e.g., TiO_2 or Fe_2O_3) and nonactive (e.g., MgO and Al_2O_3) oxide supports have been measured [9], with a superior ability to attract and activate molecular oxygen for the former ones. Recently, theoretical studies have indicated that different reaction mechanisms are dominating in the two cases [13–16]. Due to the weak O_2 binding, it has been suggested that the reaction mechanism for CO oxidation involves the formation of intermediate $CO \cdot O_2$ complexes, prior to the oxidation of the CO molecule and CO_2 formation [12,13,22]. On a nonactive support material, an Eley–Rideal reaction mechanism for CO oxidation at the Au/MgO perimeter has been proposed, showing low reaction barriers for both $CO \cdot O_2$ and the subsequent CO_2 formation [13,14]. In contrast, studies of this reaction at the Au/TiO_2 perimeter reveal that a Langmuir–Hinshelwood mechanism is possible, mainly because of the increased ability of the support to attract and activate oxygen molecules [15,16]. However, common for both cases is the active character of low-coordinated Au atoms at the Au/support perimeter interface.

For the supported Au systems, one rather unexplored topic is the influence of coadsorbates on the catalysts' per-

* Corresponding author.
E-mail address: p.broqvist@fy.chalmers.se (P. Broqvist).

0021-9517/$ – see front matter
doi:10.1016/j.jcat.2004.07.009

formance. The activity for CO oxidation has been shown to depend crucially on the catalyst preparation. In particular, the activity is sensitive to traces of chlorine, left from the catalyst synthesis when using, e.g., $HAuCl_4$ as precursor. The poisonous effect of Cl is believed to be twofold [23]: First, during the calcination of the prepared catalyst, Cl enhances sintering of Au particles. Secondly, Cl hinders reactant adsorption by site blocking and/or by long-ranged electrostatic interactions. Furthermore, electronic effects could be important, where Cl drain electrons from the Au particle. The site-blocking scenario is supported by measurements of an activity suppression for the CO oxidation reaction at a Cl/Au molar ratio even as low as 0.0006 [23]. The electronic effect modifies the activation of adsorbed reactants, and especially the activation of the adsorbed O_2 molecules, where the formation of a superoxo or a peroxo ion is crucial for the continuous reaction. In contrast to Cl, other coadsorbates could act as promoters. For example, Häkkinen et al. [6] have recently studied the effect of adding an electron donor (Sr) to small MgO-supported Au clusters. It was found that the addition of Sr significantly increases the amount of CO_2 produced per deposited cluster. This was explained by enhanced adsorption and activation of O_2 on the Sr-doped systems.

In this paper, we use a first-principle technique to study the effect of adding either Cl (a one-electron acceptor) or Na (a one-electron donor) to a model Au/MgO catalyst. By using two different catalyst modifiers, we are able to study both poisoning and promoting effects within the same computational scheme. Several aspects regarding the catalytically activated CO oxidation reaction will be considered, including adsorption of Cl/Na on the Au/MgO model system, coadsorption of CO and O_2 together with Cl/Na, and $CO + O_2$ reaction in the presence of Cl/Na. The selection of MgO as support is based on two considerations: First, the structural simplicity of MgO reduces the size of the model systems, allowing for an extensive study. Second, the effects due to the poisoning or promotion of the Au nanoparticles by themselves are expected to be largest on a nonactive material as MgO.

2. Computational method

All calculations are performed using the density-functional theory (DFT) in the implementation with plane waves and ultrasoft pseudopotentials [24]. The results are obtained in the GGA-RPBE density-functional formalism [25]. RPBE is known to improve the description of molecules and the adsorption of molecules on surfaces over other GGA formulations [25]. More specifically, we believe that the binding of oxygen to gold is better described with this functional, as it reduces the overbinding found with other GGAs [26]. Nonlocal ultrasoft pseudopotentials [27] have been used to describe the interaction between the valence electrons and

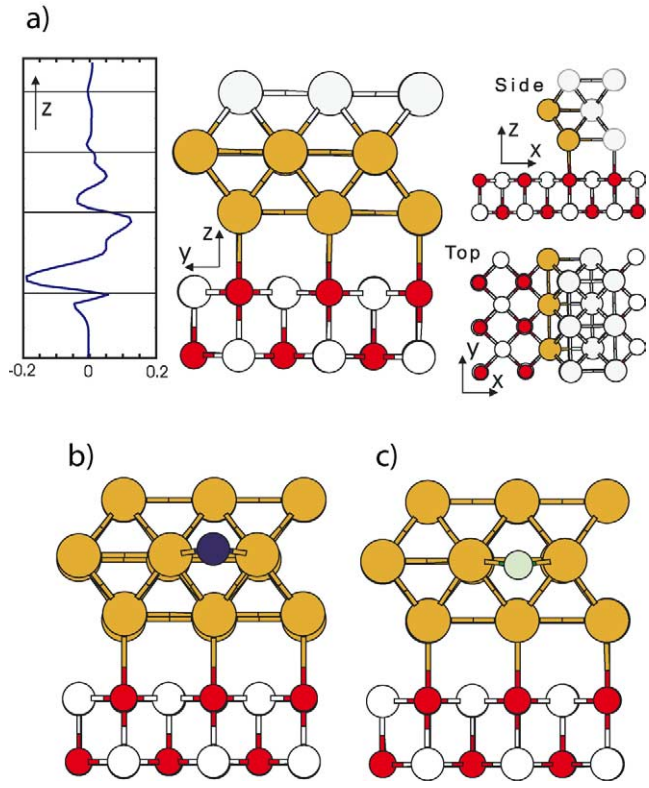

Fig. 1. (a) Front, side, and top view of the used Au/MgO model catalyst. In this figure, the Au atoms kept frozen in the model are for clarity colored white. The integrated charge difference calculated from $\delta\rho(z) = \int(\rho_{Au/MgO} - \rho_{Au} - \rho_{MgO})dxdy$ is given in units of $e^-/Å$. (b) Front view of Na adsorption on a bridge Au–Au site. (c) Front view of Cl adsorption on a bridge Au–Au site.

the core electrons.[1] The cutoff energy for the expansion of the electronic wavefunctions was set to 25 Ry.

The model consists of a Au rod supported on a perfect MgO(100) surface (discussed further below). Two different unit cells have been used, namely the $p(4 \times 3)$ and the $p(4 \times 4)$ unit cells for the MgO(100) surface, cf. Fig. 1. The large size along the x direction ensures a small interaction between periodically repeated Au rods, as they are separated by more than 6 Å. All calculations reported refer to the $p(4 \times 3)$ unit cell unless the use of the $p(4 \times 4)$ unit cell is stated. The lattice constant for the geometry optimized bulk MgO (4.30 Å) has been used for the construction of the model. The Au rod is created by geometry optimization of a 3-layers-thick Au film on top the MgO(100) surface (kept fixed), and then removing atom by atom to create the desired Au/MgO model. The Au–Au bond length is thus strained in the x–y directions to some extent compared to Au bulk (the Au/MgO lattice mismatch is $\sim 3\%$), while the interlayer distance is slightly reduced. For the continuous study, the back of the Au rod is kept fixed to simulate a nanoparticle edge (see Fig. 1a), as well as the MgO(100)

[1] Number of electrons treated explicitly are: Mg(2), O(6), C(4), Na(1), Cl(7) and Au(11).

Table 1
Calculated and experimental [33] bond lengths (d) and binding energies (D) of some relevant diatomic molecules

	d_{calc} (Å)	d_{exp} (Å)	D_{calc} (eV)	D_{exp} (eV)
Na_2	3.11	3.06	0.79	0.71
Cl_2	2.00	1.99	2.54	2.48
O_2	1.24	1.21	5.50	5.12
CO	1.16	1.13	10.94	11.10

surface. Fixing atoms will affect the absolute values for the calculated adsorption energies to some extent. However, for MgO, surface relaxation is minimal [28], and error cancellation enables us to make accurate comparisons between adsorption energies calculated for the different scenarios investigated. A 10 Å vacuum width is used together with a dipole layer, to correct the differences in work function between the two slab surfaces. Depending on the length of the model Au rod, either 1×4 (for the $p(4 \times 3)$ cell) or 1×2 (for the $p(4 \times 4)$ cell) rectangular k-point sampling grids were employed. With this computational setup, the adsorption energy of CO to the clean Au model is converged to within 0.05 eV. The structural relaxation is performed using the Broyden–Fletcher–Goldfarb–Shanno (BFGS) algorithm [29]. The geometries are converged when the residual force on the moveable atoms is less than 0.05 eV/Å and when the change in absolute energy is less than 1×10^{-4} eV.

The computational scheme has been tested by calculating the bond lengths and bond strengths of some relevant diatomic molecules (Table 1). The agreement with experimental values is good. We also find a good performance of the computational setup on the evaluation of MgO and Au bulk properties (lattice parameters of 4.30 and 4.22 Å, only 2–3% larger than the experimental values).

Reaction barriers are calculated by constraining a chosen reaction coordinate, e.g., in the case of $CO \cdot O_2$ formation the O_2–CO distance, and then allowing the atoms to relax under this constraint. The reaction barrier is found at the maximum of the calculated potential energy curve as a function of the introduced constraint. It was checked that continuous reaction paths were obtained by plotting the energy versus the integrated displacements of the whole system.

Some of us have previously studied the $CO + O_2$ reaction at similar Au/MgO model systems [13,14], finding somewhat lower adsorption energies than reported herein. This is due to the choice of a thinner Au rod together with a lower adsorbate coverage in the present study. Qualitatively, however, our results for the clean Au edge are in agreement with Refs. [13,14].

3. Model systems: Au/MgO, Na/Au/MgO, and Cl/Au/MgO

Different aspects of modeling Au/MgO interface boundaries have been discussed in Refs. [13,14]. In this study, the main focus is on the CO oxidation reaction over a modified Au/MgO model catalyst. The aim is to explore the effect of coadsorbates on the stabilities of the involved species and activation energy for the $CO + O_2$ reaction. As mentioned in Section 1, both a single electron donor (Na) and a single electron acceptor (Cl) are used as catalyst modifier. The model catalyst systems are shown in Fig. 1. Fig. 1a shows the clean Au/MgO model, similar to the "Type II" interface in Refs. [13,14] displaying the lowest activation energy barrier for the CO oxidation reaction, using an Eley–Rideal type of mechanism. The model can be regarded as resulting from the formation of a truncated Wulff polyhedron, and consists of a Au rod (continuous in the y direction) supported on a perfect MgO(100) surface. The election of this model relies on the fact that a majority of the catalytically active sites around a nanometer-sized particle are described by it. In Refs. [13,14] the unreactive character of Au(100) and Au(111) facets was demonstrated, as well as the enhanced activity of low-coordinated corner sites. However, given the low abundance of this type of sites for a 2- to 3-nm Au particle, and the difficulties of treating them in our computational setup (as they require the use of a much larger model like the Au_{34} cluster used in Ref. [14]) we will not discuss them in this paper. The interaction between the Au rod and the MgO support involves a partial charge transfer from the support to the metal, as displayed in the charge difference plot in Fig. 1a. The charge difference is most evident in the interfacial region, in line with previous observations of MgO-supported metal particles [13,14,28,30–32]. The binding of the Au particle to the MgO(100) surface can be characterized as a polarization bond.

When adding Na to the Au/MgO model, charge is transferred from the Na adsorbate to the Au rod. The Na–Au interaction is ionic and a long bond distance is calculated between Na and the Au edge (2.93 Å to the closest Au atom, 2.52 Å to the Au rod). The adsorption potential energy for Na bonded to the Au rod is calculated to -2.19 eV/Na in the most stable adsorption configuration, depicted in Fig. 1b. Adsorption energies calculated for Na adsorption at different sites on the edge, i.e., first and second row of Au, are nearly degenerated (within ~ 0.05 eV). Decreasing the Na coverage using a $p(4 \times 4)$ unit cell slightly increases the adsorption energy (-2.26 eV/Na). The Na–Au bond is considerably stronger than the binding energy in the Na_2 dimer, cf. Table 1. These results suggest that clustering of Na at the Au edge should not occur, as the positively charged Na ions will repel each other at the edge. This scenario is supported by calculations at a higher Na coverage. Having two Na atoms in the $p(4 \times 3)$ unit cell results in an adsorption potential energy of -2.11 eV/Na and an optimized Na–Na distance of 3.65 Å. In this case, the adsorbed Na atoms are in a slightly off-bridge position (Au–Au distance is 3.04 Å).

Experimentally, alloying of Na and Au has been observed at high Na coverages [34]. At lower coverage ($\theta \sim 0.6$ ML) and low temperatures, Na adatoms can form a physical Na overlayer corresponding to a Na–Na next nearest neighbor distance of 3.75 Å [34]. This distance is similar to what

we calculate at the Au edge in the case of high coverage (3.65 Å). To investigate the stability of Na adatoms on Au surfaces, calculations have been performed where a Na atom was placed on a Au(111) surface (modeled by a 4-layer slab in a $p(2 \times 2)$ unit cell), either as an adatom or mixed into the first or second Au layer. We find that it is favorable by ~ 0.2 eV to swap the positions of a Na adatom and a surface Au atom. Moreover, having Na in the second atomic layer is even more stable (by ~ 0.2 eV). Thus, thermodynamically, a small driving force exists for Na atoms to diffuse into the Au bulk. Explicit calculations show that the same situation applies for the Au edge. Furthermore, recent calculations indicate that Na^+ ions can bind strongly to the MgO(100) terrace [35]. Thus, migration of Na^+ ions from the Au nanoparticle to the MgO support could be a possible situation. However, as mentioned above, from our calculations there is no additional energy gain when the Na atom is adsorbed over a surface O^{2-} site close to the Au edge compared to the configuration displayed in Fig. 1b. Consequently, Na adatoms correspond to a metastable situation which could be created, for example, by doping preformed Au catalysts with small amounts of Na. However, careful preparation methods to avoid alloying seem mandatory.

For Cl, adsorption energies are higher. Cl binds with an adsorption potential energy of -2.60 eV/Cl in the configuration shown in Fig. 1c. The bond distances between Cl and the Au rod are shorter (2.56 Å to closest Au atom, 2.00 Å to the Au rod) than the distances reported for Na. Similar to the Na adsorption, the adsorption energy is slightly increased when decreasing the Cl coverage (-2.66 eV/Cl) using the $p(4 \times 4)$ unit cell. The Cl–Au binding energy is almost twice the binding energy calculated for the Cl_2 molecule (cf. Table 1). Adsorption in a bridge site is calculated to be ~ 0.2 eV more stable than is adsorption atop Au or closer to the support material.

Further characterization of the adsorption of Na and Cl can be obtained by calculating the induced dipole moment from

$$\Delta\mu = \int x\Delta\rho(x)\mathrm{d}x, \tag{1}$$

where

$$\Delta\rho(x) = \int (\rho_{\mathrm{X/Au/MgO}} - \rho_{\mathrm{Au/MgO}} - \rho_{\mathrm{X}})\mathrm{d}y\mathrm{d}z,$$
$$\mathrm{X} = \mathrm{Na},\ \mathrm{Cl}. \tag{2}$$

ρ is the electron density and the adsorbates are positioned at lower x values relative the Au rod. $\Delta\mu$ is calculated to 2.78 and -1.00 D (1 D $= 3.336 \times 10^{-10}$ C m [33]) for the Na and Cl system, respectively. In a simplistic model, these values infer a work-function decrease in case of Na adsorption corresponding to a charge donation from the adatom to the substrate, while for the Cl adsorption, a small work-function increase is expected together with a negatively charged Cl ion.

4. Adsorption of reactants

In this section, the relevant steps preceding the actual CO oxidation reaction are discussed. The main focus is on relative stabilities among the reacting adsorbates, CO and O_2, adsorbed at the modified Au/MgO edge.

4.1. Molecular and atomic adsorption of oxygen

4.1.1. Molecular adsorption

From experiment and theory, the interaction of molecular oxygen with Au single crystals is known to be weak [17–21]. In contrast, based on thermal desorption data assuming first-order desorption, Stiehl et al. [36] have recently reported a binding energy of 0.35 eV for the adsorption of O_2 on TiO_2-supported Au. Increased affinity of O_2 for nanosized Au particles has previously been suggested [5,11,12,20,21].

The most stable adsorption site for O_2 on the clean Au/MgO model is in a bridge position with the O_2 molecule parallel to the Au edge (cf. Fig. 2a) giving a weak adsorption potential energy of -0.13 eV. The adsorption of the O_2 molecule is accompanied by a decreased magnetic moment from $2\mu_B$, calculated for the isolated O_2 molecule, to $1.20\mu_B$. This infers that the adsorbed O_2 is in a superoxo-

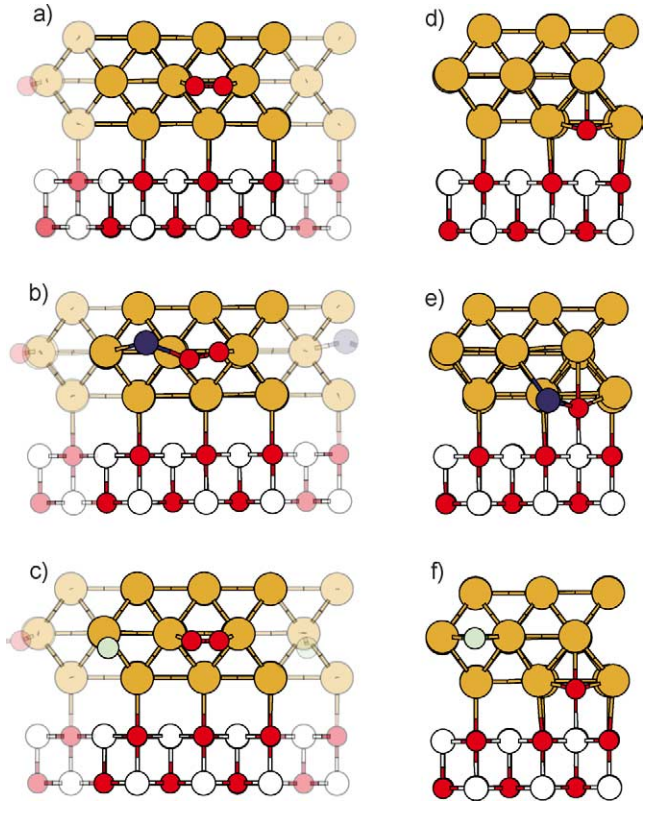

Fig. 2. Front view of the stable configuration for O_2 adsorption on (a) the Au/MgO model catalyst, (b) the Na-decorated edge, and (c) the Cl-decorated edge. Front view of atomic O adsorption on (d) the Au/MgO model catalyst, (e) the Na-decorated edge, and (f) the Cl-decorated edge. Transparent parts are the periodic repetitions inserted for further clarification of the model.

like state (O_2^-). This is also seen in the O–O bond length, which is calculated to be 1.31 Å. The formation of a superoxo ion prior to O_2 dissociation has been found earlier in theoretical studies of O_2 adsorption on Pt(111) [37].

Molecular oxygen adsorption on the Na-decorated Au edge is associated with a potential energy of −0.33 eV. The most stable adsorption configuration is displayed in Fig. 2b. The origin of the enhanced adsorption energy is the formation of a Na–O_2 chemical bond together with the additional electron provided by the Na atom, leading to a higher charge donation capability from the Au rod to the O_2 molecule. The larger amount of charge transferred to O_2 is reflected in a lowering of the magnetic moment ($0.67\mu_B$) together with an elongation of the O–O bond length (1.37 Å) for the adsorbed O_2. These results suggest that a superoxo ion is formed at the Na-decorated edge. This behavior should be similar when adding other types of electron donors, cf. Ref. [6].

At the Cl-decorated Au edge, no stable oxygen adsorption site is found for the $p(4 \times 3)$ unit cell. The adsorption potential energy is calculated to +0.20 eV for the most stable configuration, displayed in Fig. 2c. This can be rationalized by the fact that in this case, two electrons need to be subtracted from the Au rod, forming Cl^- and O_2^-. A sign of decreased charge transfer to the O_2 molecule is the calculated magnetic moment, which now becomes $1.33\mu_B$. The O_2 bond length is 1.28 Å, again demonstrating the lower capability of charge donation for the Cl-decorated edge. Moreover, the repulsive Coulomb interaction between O_2 and Cl forces the Cl atom to an unfavorable atop site. To investigate the range of the poisoning effect of Cl, calculations with a lower Cl coverage were made using the $p(4 \times 4)$ unit cell. Owing to the larger unit cell, Cl is able to remain adsorbed on a bridge site upon O_2 adsorption, and the O_2 adsorption is therefore stabilized slightly, the adsorption potential energy becoming +0.02 eV, i.e., still endothermic. Thus, the poisonous effect of Cl toward O_2 adsorption does not only affect the closest adsorption sites but also at least two bridge sites further. The results for oxygen adsorption are summarized in Table 2.

4.1.2. Atomic adsorption

The most stable configuration for the adsorption of atomic oxygen on the clean Au model is found at the lower Au edge, on top of a Mg^{2+} cation (see Fig. 2d). This is understandable, as it represents epitaxial growth of O^{2-} on the MgO surface. The structure is depicted in Fig. 2d. The adsorption potential energy with respect to gas-phase molecular oxygen is calculated to −0.13 eV/O, meaning that dissociation of adsorbed O_2 is thermodynamically favorable at the Au edge. However, the dissociation barrier on a similar system is high (∼ 1.7 eV using RPBE in the most favorable case [14]). High barriers have also been calculated for small Au cluster anions [38].

For the adsorption of atomic oxygen on the Na-decorated edge, two different cases were studied: with and without the formation of a Na–O chemical bond. The adsorption potential energies calculated for the two cases were −0.84 and −0.07 eV/O, respectively. As was the case with the molecular oxygen, a large energy gain is associated with the formation of a Na–O bond. The most stable configuration is displayed in Fig. 2e. Also, comparison with molecular adsorption at the Na-decorated edge reveals that dissociative adsorption of oxygen is a thermodynamically more stable situation.

The atomic oxygen adsorption on the Cl-decorated Au edge displays similar energetics as for the clean Au edge. Also in this case, two different Cl–O adsorption configurations were investigated. The adsorption potential energies were calculated to −0.03 and −0.13 eV/O for the nearest and next-nearest neighbor Cl–O configurations, respectively. The next-nearest neighbor adsorption energy is the same as the one calculated for the clean edge, indicating that the electronic effect of the Cl interaction to the Au rod has small effect on the adsorption energy of the atomic oxygen. The most stable adsorption configuration found is displayed in Fig. 2f.

Table 2
Calculated adsorption potential energies for O_2, O, and CO on the modified and unmodified Au/MgO models

	Au/MgO (eV)	Na/Au/MgO (eV)	Cl/Au/MgO (eV)
O_2	−0.13	−0.33	+0.20
O	−0.13	−0.84 (−0.07)	−0.03 (−0.13)
CO	−0.75	−0.52	−0.60

For atomic oxygen, the adsorption energies for both nearest and next-nearest (in parentheses) neighbor are given. All results are calculated in the $p(4 \times 3)$ unit cell. The atomic oxygen adsorption energy is calculated with respect to gas-phase O_2.

4.2. CO adsorption

CO adsorption on late transition metal surfaces can be described by the Blyholder model [39–42]. In this model, the CO molecule adsorbs by donating its 5σ lone electron pair into empty states of the metal d band together with backdonation from the metal d band to the antibonding $2\pi^*$ orbital on the CO molecule. The backdonation decreases the bond strength in the CO molecule and prepares the adsorbed CO for reaction with oxygen to form CO_2.

The energetics for the CO adsorption on the three models are reported in Table 2. Binding of CO at the clean Au edge leads to an adsorption potential energy of −0.75 eV while adsorbing CO at the Na- and Cl-decorated edges yields an adsorption potential energy of −0.52 and −0.60 eV, respectively. The CO binds atop an edge Au atom as depicted in Fig. 3 for the three models. Decreasing the coverage, i.e., increasing the unit cell to a $p(4 \times 4)$ unit cell, has very little effect on the CO-adsorption energy (0.02 eV in the case of the Cl-decorated edge). Thus, lateral repulsive electrostatic interactions should not be the cause for the decrease in CO adsorption energy. Using the d-band model [43], these adsorption energies suggest that the d-band center is shifted

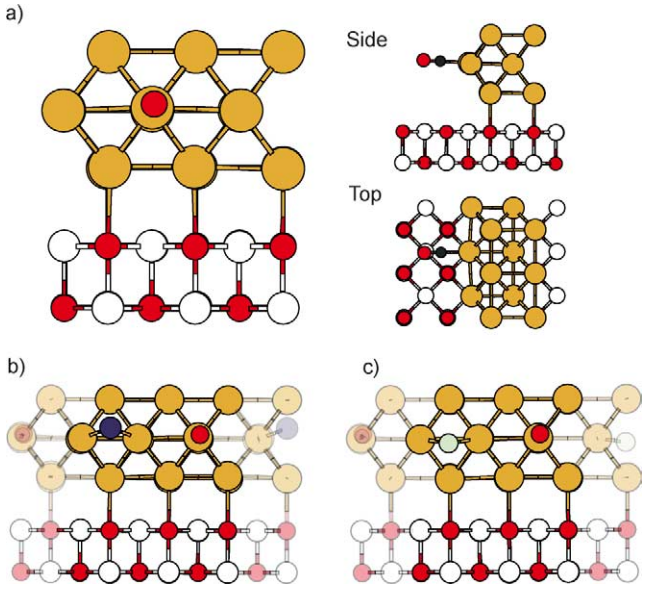

Fig. 3. (a) Front, side, and top view of the stable configuration for CO adsorption on the Au/MgO model catalyst. (b) Front view of CO adsorption on the Na-decorated edge. (c) Front view of CO adsorption on the Cl-decorated edge.

toward lower energies in the DOS upon Na and Cl adsorption. For CO adsorption on Pt, a linear relationship between the CO adsorption energy and the d-band center has been observed [43]. For the models studied here, we observe a small lowering of the d-band center with respect to the Fermi level, calculated to −0.09 and −0.06 eV, for the Na- and Cl-decorated Au/MgO models, respectively, compared to the clean Au/MgO model. The trend in the d-band center shift is consistent with the observed lowering in adsorption energy for CO adsorption at the Na- and Cl-decorated edges. Finally, in all cases a small elongation (≈ 0.5–1.0%) of the C–O bond length is found upon adsorption, indicating some occupation of the CO $2\pi^*$ orbital and the existence of a weak backdonation bond according to the Blyholder model discussed above.

4.3. Coadsorption of CO and O_2

As already mentioned, and in agreement with other studies of the CO + O_2 reaction over Au-based catalysts [12–14, 22], the affinity toward oxygen for the Au/MgO model catalyst is low. Therefore, the CO oxidation reaction most likely involves some kind of intermediate complex of CO and O_2. In Refs. [13,14], a particular stable configuration of CO and O_2 coadsorbed at the perimeter of an Au/MgO catalyst was found, with a low barrier of formation. The stability of such a complex will be even more important when Cl is introduced in the system, due to the lowering of the oxygen adsorption energy. Therefore, the stability of the CO · O_2 complex is investigated in the presence of Na and Cl. An important criterion for discussing feasible reaction pathways is that the stability of the formed CO · O_2 complex should be higher than that of CO alone.

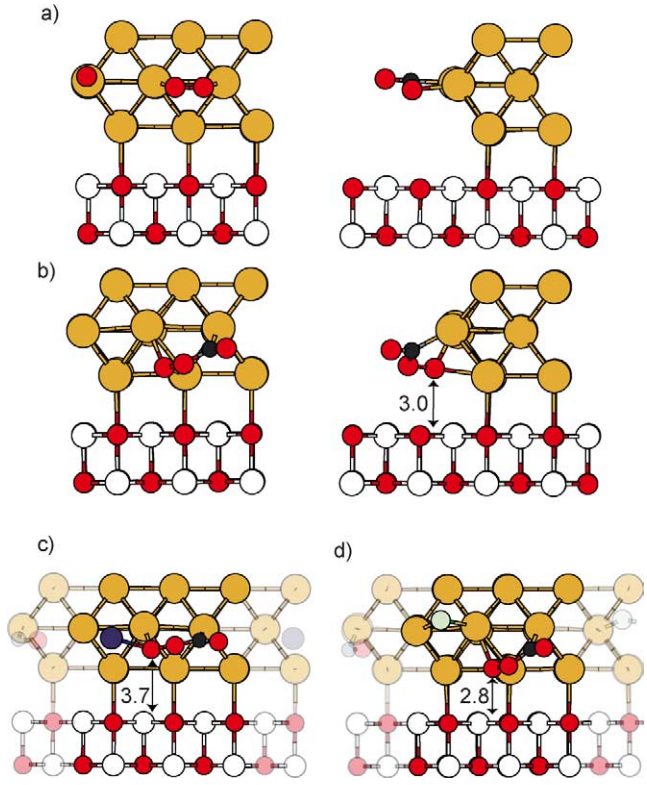

Fig. 4. (a) Front and side view for simultaneous adsorption of CO and O_2 in the stable configurations displayed in Figs. 2 and 3 for the clean Au edge. (b) Front and side view of the stable CO · O_2 complex on the clean Au edge. (c) Front view of the CO · O_2 complex on the Na-decorated edge. (d) Front view of the CO · O_2 complex on the Cl-decorated edge. The distances between the oxygen molecule and the support for the different CO · O_2 configurations are given in Å. The O–O bond length is 1.34 Å in (a) and ∼ 1.47 Å in (b), (c) and (d).

First, coadsorbing CO and O_2 in the stable configurations discussed previously was tested on the bare Au/MgO edge (cf. Fig. 4a). The adsorption potential energy for both CO and O_2 is calculated to −0.71 eV, which should be compared to the adsorption energy for the CO alone (−0.75 eV) and the sum of CO alone and O_2 alone, −0.88 eV ($E_{\text{ads}}^{\text{CO}} + E_{\text{ads}}^{\text{O}_2}$) at the lower coverage (cf. Table 2). Consequently, molecular O_2 adsorption is not enhanced by prior CO adsorption. The situation is different when a CO · O_2 complex is formed; on the bare Au/MgO model catalyst, the CO · O_2 complex adsorption potential energy is calculated to −0.90 eV, which gives a 0.15 eV energy gain compared to the adsorption of CO alone and having O_2 in gas-phase. The adsorption configuration is displayed in Fig. 4b. Decreasing the coverage using the $p(4 \times 4)$ unit cell increases the adsorption energy slightly (−0.98 eV). The binding of the CO · O_2 complex can be understood as a peroxo-like O_2 (with a O–O bond length of 1.47 Å and no magnetic moment) and an activated CO.

The adsorption potential energy calculated for the CO · O_2 complex adsorbed on the Na-decorated Au edge is −1.62 eV. This is almost twice the adsorption energy calculated for the CO · O_2 complex on the clean Au edge. From the analysis of the adsorption configuration (displayed in Fig. 4c), it is con-

cluded that the reason for the increased stability is the formation of a Na–O_2 bond, as was also the case for the molecular and atomic oxygen adsorption. The location of the CO · O_2 complex is moved up to be parallel to the Au edge, while the complex in the case of the clean Au edge was formed closer to the MgO(100) surface. To test the effect of removing the Na–O_2 chemical interaction, we calculated the adsorption of the CO · O_2 complex in the $p(4 \times 4)$ unit cell. In this larger cell, the adsorption potential energies with either direct Na–O_2 contact or no contact are −1.42 and −0.86 eV, respectively. Thus, the increased stability is mainly due to the formation of a direct chemical bond between the Na ion and the O_2 molecule, with the enhancement effect of Na being short ranged.

The formation of the CO · O_2 complex on the Cl-decorated Au edge is less energetically favorable than in the former cases. In fact, the CO · O_2 complex is less stable (adsorption potential energy of −0.49 eV) than CO alone (−0.60 eV) on the Cl-decorated edge. The relaxed structure is displayed in Fig. 4d. The low adsorption energy is in line with the results obtained for adsorption of molecular oxygen. As for O_2, the effect of Cl coverage was studied by using the $p(4 \times 4)$ unit cell. Two different scenarios were investigated, one with the same Cl–CO · O_2 distance as in the $p(4 \times 3)$ cell, and another with Cl moved to the next bridging Au–Au site on the edge. The adsorption potential energies for the CO · O_2 complex are −0.46 and −0.67 eV, respectively. Even at the furthest distance from Cl, the stability of the CO · O_2 complex decreases by ∼ 0.3 eV with respect to the clean edge. This highlights the long-range poisonous effects of Cl already discussed in the case of O_2 adsorption. Table 3 summarizes the energetics for the CO · O_2 complex formation on all systems.

One often discussed issue is the role played by the support material for the activity of Au particles. To investigate this and study whether the MgO substrate acts differently when Na or Cl is coadsorbed with the CO · O_2 complex at the Au edge, we have calculated the induced charge density due solely to the interaction between the CO · O_2 complex and the MgO support. Following Refs. [13,14], such MgO-induced charge density is defined as

$$\Delta\rho = \rho_{\mathrm{CO{\cdot}O_2/X/Au/MgO}} - \rho_{\mathrm{CO{\cdot}O_2/X/Au}} - \rho_{\mathrm{X/Au/MgO}} + \rho_{\mathrm{X/Au}} \quad (3)$$

and is obtained as the difference between the induced charge densities for CO · O_2–Au/MgO and Au/MgO (in our notation, the extra symbol "X" has been added, labeling either Na or Cl dopants). The results are reported in Fig. 5. The plots are 2D representations, meaning that the charge differences are integrated in the y direction and projected in the x–z plane. For all the models, we observe a charge depletion from a region close to the support and a charge accumulation at the O_2 part of the CO · O_2 complex. There are, however, important differences between the three cases. The density difference is similar for the clean edge as for the Cl-decorated edge, suggesting similar stabilization of the complex from the MgO support without or in the presence

Table 3
Coverage dependence on the stability of the CO · O_2 complex

	$p(4 \times 3)$ (eV)	$p(4 \times 4)$ n (eV)	$p(4 \times 4)$ nn (eV)
Au/MgO	−0.90	–	−0.98
Na/Au/MgO	−1.62	−1.42	−0.86
Cl/Au/MgO	−0.49	−0.46	−0.68

n is nearest neighbor to the O_2 molecule, nn is next-nearest neighbor to the O_2 molecule (closer to the CO molecule). n and nn are only relevant for the Na- and the Cl-decorated edges.

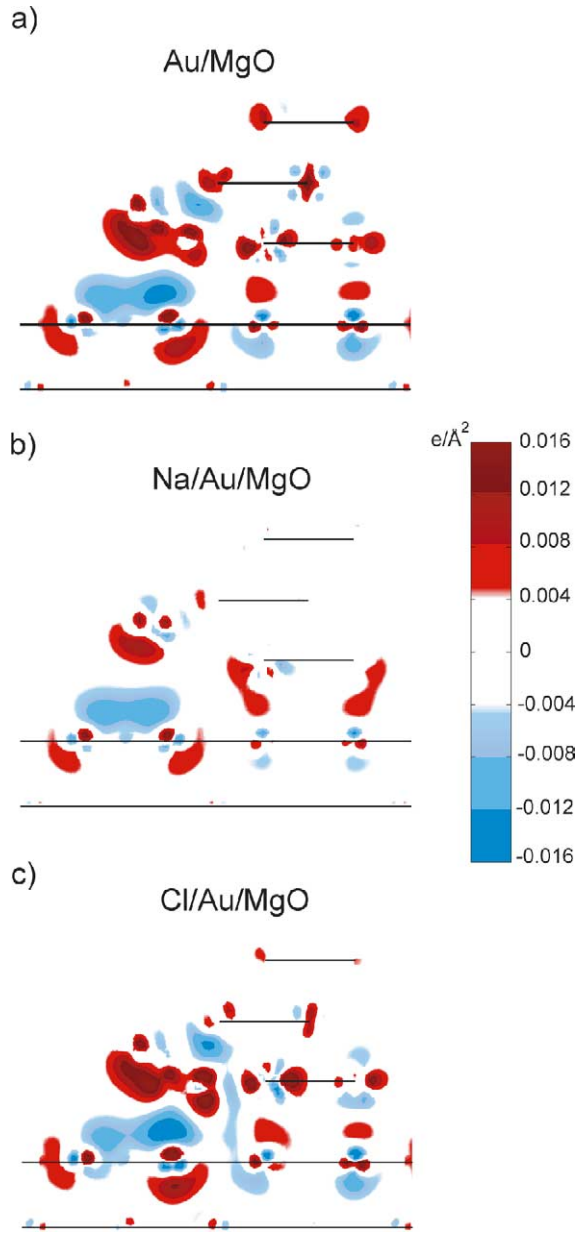

Fig. 5. 2D plots showing the MgO-induced charge density, calculated from Eq. (3) (integrated along y projected in the x–z plane), for the CO · O_2 formation on (a) the clean Au/MgO, (b) the Na-decorated Au/MgO, and (c) the Cl-decorated Au/MgO edge. Unit is $e^-/Å^2$. Positions of the substrate as well as the Au layers are indicated with black lines.

of Cl. For the Na-decorated edge, the influence of the support is significantly smaller (compare (b) with (a) and (c) of Fig. 5). This is not surprising, since Na increases the charging the O_2 part of the complex making the charge transfer from the substrate unnecessary.

5. CO oxidation reaction

Having established the adsorption energetics for the involved reactants, we now continue with the actual CO oxidation reaction. To close the catalytic cycle, the important following oxygen abstraction reaction step will also be considered subsequently.

5.1. $CO + O_2$ reaction

Following the work in Refs. [13,14], the most plausible reaction pathway for CO oxidation on these model systems consists of two reaction steps. Starting with preadsorbed CO on the edge, we have first the $CO \cdot O_2$ formation. This step is followed by an elongation of the O–O bond together with CO_2 formation. The reason for a stepwise Eley–Rideal (ER) mechanism is the poor binding of molecular oxygen, together with high barriers for O_2 dissociation [13,14]. However, at the Na-decorated Au edge, other reaction steps could be of interest. The enhanced adsorption energy for the molecular oxygen together with a lowered adsorption energy for CO suggests the possibility of a second type of ER mechanism where CO directly reacts with a preadsorbed oxygen molecule.

The minimum energy paths (MEP) calculated for $CO \cdot O_2$ formation on the three different model systems are displayed in Fig. 6a. For the clean edge and the Na-decorated edge, the barrier is calculated using the $p(4 \times 3)$ unit cell. For the Cl-decorated edge, the $p(4 \times 4)$ unit cell is used because the $CO \cdot O_2$ formation is unstable with respect to CO adsorption in the $p(4 \times 3)$ unit cell. The initial states are CO adsorbed as in Fig. 3 and O_2 approaching from the gas phase. The final states are the intermediate $CO \cdot O_2$ complexes displayed in Figs. 4b–d.

For the clean Au edge, a barrier is found for approaching O_2. The reaction barrier for $CO \cdot O_2$ formation is calculated to ~ 0.3 eV at a O_2–CO distance of ~ 1.8 Å. For a similar reaction pathway, no reaction barrier is calculated when Na is added to the edge (cf. Fig. 6a). In this case, there is instead an attraction between Na and the O_2 molecule from the start of the reaction path, and the main reason for the nonexisting reaction barrier is the larger affinity toward oxygen for the Na-decorated edge. For the Cl-decorated edge, the barrier is similar to the one calculated for the clean edge, ~ 0.3 eV (cf. Fig. 6a). The barrier is located at a similar O_2–CO distance (~ 1.8 Å) as for the clean model. Also, the atomic configurations corresponding to the highest energy along the MEP are similar for the two cases, with O–O bond lengths of 1.32–1.33 Å and magnetic moments slightly smaller than

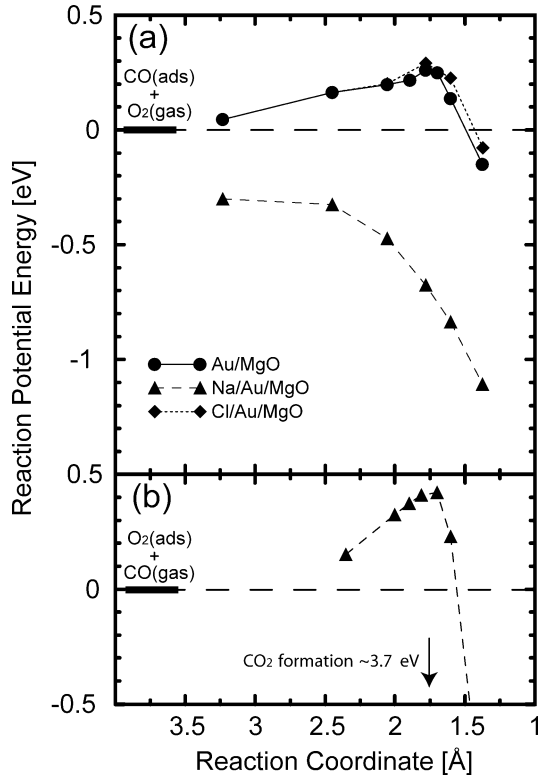

Fig. 6. (a) MEP for $CO \cdot O_2$ formation on the discussed models. The MEPs for the clean model and the Na-decorated model are calculated in the $p(4 \times 3)$ unit cell, while the barrier for the Cl-decorated edge is calculated in the $p(4 \times 4)$ unit cell. The structures for the final points are displayed in Figs. 4b–4d. (b) MEP for CO_2 formation via the second Eley–Rideal-type mechanism with O_2 preadsorbed at the Na-decorated edge. The reaction coordinate is the O_2–CO distance.

$1\mu_B$. Thus, the origin of the barrier seems to be the formation of the peroxo ion, i.e., adding the second electron on the O_2 molecule. This rationalization explains the absence of barrier in the case of the Na-decorated edge, where the additional electron can easily be provided by the Na atom.

The next step in the reaction path is to continue from the adsorbed complex with an elongation of the O–O bond and the formation of CO_2. In this case, the introduced constraint is on the O–O bond length. The reaction barrier for the O_2 bond breakage is similar for all studied cases, calculated to ~ 0.3 eV with the barrier located at a O–O bond length of ~ 1.75 Å. This is in agreement with previous studies [13, 14].

As discussed above, a second scenario could be of interest for the Na-decorated edge, with O_2 preadsorbed on the edge (and close to a Na ion) reacting with CO approaching from the gas phase. In this case, no $CO \cdot O_2$ complex formation is possible due to steric effects; i.e., the O_2 molecule blocks the adsorption site for CO. The initial configuration for this reaction is displayed in Fig. 2b and the calculated MEP is plotted in Fig. 6b. We find a barrier for direct CO_2 formation of 0.4 eV, originating from the breaking of the O–O bond (occurring at a O–O distance of ~ 1.75 Å, as above).

5.2. $CO + O_{ads}$ reaction

An efficient removal of leftover oxygen atoms from the above discussed CO oxidation reaction is important in order to close the reaction cycle and prevent oxygen poisoning. Oxygen abstraction from a similar model as the clean edge has been shown to display a very low barrier for CO_2 formation from adsorbed CO and atomic oxygen via a Langmuir–Hinshelwood (LH) mechanism [13,14]. However, for the Na-decorated edge, this step could become crucial, due to the very stable binding of atomic oxygen on this model.

Adsorbing CO on the clean model with preadsorbed oxygen (depicted in Fig. 2d) leads to similar energetics as for CO adsorption at the clean Au edge. Furthermore, the adsorption energy is similar (within 0.05 eV) for adsorption atop the Au atom above the preadsorbed oxygen atom as adsorption at neighboring Au atoms. The initial configuration used for the calculation of the reaction barrier for oxygen abstraction at the clean edge is shown as an inset in Fig. 7a. For the Na-decorated edge, an increased adsorption energy of −0.82 eV is calculated for CO on the upper Au edge, at a Au–Au bridge position close to the preadsorbed Na–O complex (see inset in Fig. 7b). As CO adsorption is slightly stronger than at the clean Au edge (−0.75 eV) (and much stronger (∼ 0.3 eV) than at the Na-decorated edge), the Na–O complex is expected to act as a CO attractor.

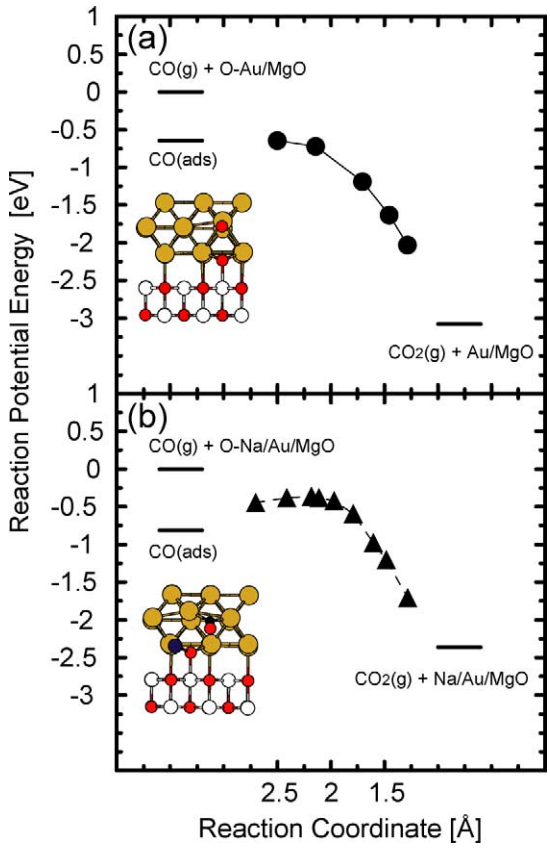

Fig. 7. Barrier for CO_2 formation on the clean O–Au/MgO model (top panel) and the O–Na/Au/MgO (bottom panel) model catalyst as a function of OC–O_{ads} distance. Front views of the initial configurations for CO adsorption are shown as insets.

The reaction barriers for the oxygen abstraction are calculated using the OC–O bond length as reaction coordinate. The MEPs calculated for the clean and Na-decorated edges are given in Fig. 7 together with the initial configurations. The barrier for the Cl-decorated edge is not included because the stability of the atomic oxygen is similar to the one calculated for the clean edge, suggesting similar barriers. For the clean edge with a preadsorbed oxygen atom, the barrier is very low (< 0.1 eV, cf. Fig. 7a). This is in agreement with previous studies [13,14] and confirms that no deactivation should occur due to leftover oxygen atoms at the Au/MgO interface. More interesting is the oxygen abstraction from the Na-decorated edge, where the stability of the oxygen atom close to a Na ion is higher. The MEP for oxygen abstraction is displayed in Fig. 7b. The calculated barrier is ∼ 0.45 eV, starting from the adsorbed CO molecule. Thus, the removal of oxygen atoms is slightly more difficult at the Na-decorated edge. However, all points on the MEP are below the reference energy for CO(g), which together with a moderate barrier and a large heat of reaction suggests that there should not be any poisoning of the catalyst due to leftover oxygen atoms.

6. Conclusion

The effect of coadsorbates (Na and Cl) on the CO oxidation reaction over a Au/MgO model catalyst has been studied using density-functional theory, investigating both promoting and poisonous effects. The interaction between Na and Cl with the Au/MgO catalyst is found to be strong. Charge transfer is observed between the Au metal and the coadsorbates, indicative of an ionic binding forming a $Na^{\delta+}$ and a $Cl^{\delta-}$ upon adsorption. The formation of charged adatoms prevents clustering at the edge. For Na, a more critical problem is to avoid alloying with Au as well as migration of Na^+ ions to the MgO support; the results of test calculations suggest that special care during the preparation of a promoted catalyst is needed.

For the binding of CO to the modified catalysts, there is relatively little influence of either Cl or Na; on the contrary, in the case of O_2 the influence is drastic, with Cl clearly acting as a poison and Na acting as a promoter. The reason for this is the sensitivity of the O_2 binding to the presence of electronic charge available to be transferred to the molecule. Interestingly, we find the promoter effect of Na to be local, while the poisonous effect of Cl is long ranged. This is understood from the fact that the poisonous effect of Cl is electrostatic, and thereby declining as a power law, while the promoting effect of Na requires overlap of orbitals and the creation of a chemical bond.

Similar poisoning/promoter effects occur for the formation of a $CO \cdot O_2$ complex at the Au/MgO perimeter. The

stability of such a complex is significantly enhanced at the Na-decorated Au edge compared to the clean edge. The enhancement is mainly due to the formation of a Na–O_2 bond. Furthermore, the increased affinity toward oxygen for the Na-decorated edge leads to a barrier-free path for the formation of the $CO \cdot O_2$ complex. For the Cl-decorated edge at the higher coverage, formation of the $CO \cdot O_2$ complex is unlikely since it is less stable than CO adsorbed plus O_2 in the gas phase. Subsequent CO_2 formation from the formed complex has a moderate activation barrier of ~ 0.3 eV for all models. Due to the higher affinity toward O_2 at the Na-decorated edge, a second Eley–Rideal mechanism was considered, using preadsorbed O_2 and CO approaching from the gas phase. In this case, a direct CO_2 formation is possible with a reaction barrier of ~ 0.4 eV, without the formation of a $CO \cdot O_2$ complex. To complete the reaction cycle, also barriers for leftover oxygen abstraction have been calculated. These calculations show that at the clean edge, atomically adsorbed oxygen can be easily removed by CO, with very small or no reaction barriers (< 0.1 eV). At the Na-decorated edge, abstraction of atomic oxygen is slightly more difficult (0.45 eV activation barrier), but still feasible at moderate temperatures.

To conclude, the activity of CO oxidation over Au/MgO is predicted to be significantly increased by providing an "oxygen attractor", in this case Na, which results in very low barriers for the $CO + O_2$ reaction via Eley–Rideal type of reaction mechanism. The activation of O_2 at the Na-decorated edges is similar to what has been reported for O_2 adsorption on Au supported on more active support materials like TiO_2. The poisonous effects of Cl have also been investigated, finding that they extend at least two bridge sites away from the Cl. The poisoning is mainly observed in a decreased stability of the adsorbates. The reaction barrier for, e.g., the $CO \cdot O_2$ complex formation at the lower coverage seems not to be affected. Thus, the poisonous effect seems to be of site-blocking character together with long-ranged Coulomb repulsion rather than electronic.

Acknowledgments

NORFA is gratefully acknowledged for financial support (P.B.) (030449). So is the Danish Research Councils and Dansk Center for Scientific Computing (L.M.M. and B.H.).

The Competence Centre for Catalysis is hosted by Chalmers University of Technology and financially supported by the Swedish Energy Agency and the member companies AB Volvo, Saab Automobile Powertrain AB, Johnson Matthey CSD, Perstorp AB, Akzo Nobel Catalyst, AVL-MTC AB, and the Swedish Space Corporation.

References

[1] B. Hammer, J. Nørskov, Nature 376 (1995) 238.
[2] M. Haruta, T. Kobayashi, N. Yamada, Chem. Lett. 2 (1987) 405.
[3] M. Haruta, J. Catal. 178 (1997) 566.
[4] M. Valden, X. Lai, D.W. Goodman, Science 281 (1998) 1647.
[5] A. Sanchez, S. Abbet, U. Heiz, W.D. Schneider, H. Häkkinen, R.N. Barnett, U. Landman, J. Phys. Chem. A 103 (1999) 9573.
[6] H. Häkkinen, S. Abbet, A. Sanchez, U. Heiz, U. Landman, Angew. Chem. Int. Edit. 42 (2003) 1297.
[7] J. Hagen, L.D. Socaciu, M. Elijazyfer, U. Heiz, T.M. Bernhardt, L. Wöste, Phys. Chem. Chem. Phys. 4 (2002) 1707.
[8] W.T. Wallace, R.L. Whetten, J. Am. Chem. Soc. 124 (2002) 7499.
[9] M.M. Schubert, S. Hackenberg, A.C. van Veen, M. Muhler, V. Plzak, R.J. Behm, J. Catal. 197 (2001) 113.
[10] A. Wolf, F. Schüth, Appl. Catal. A 226 (2002) 1.
[11] N. López, J.K. Nørskov, J. Am. Chem. Soc. 124 (2002) 11262.
[12] Z.-P. Liu, P. Hu, A. Alavi, J. Am. Chem. Soc. 124 (2002) 14770.
[13] L.M. Molina, B. Hammer, Phys. Rev. Lett. 90 (2003) 206102.
[14] L.M. Molina, B. Hammer, Phys. Rev. B 69 (2004) 155424.
[15] Z.-P. Liu, X.Q. Gong, J. Kohanoff, C. Sanchez, P. Hu, Phys. Rev. Lett. 91 (2003) 266102.
[16] L.M. Molina, M.D. Rasmussen, B. Hammer, J. Chem. Phys. 120 (2004) 7673.
[17] D.A. Outka, R.J. Madix, Surf. Sci. 179 (1987) 351.
[18] D.H. Parker, B.E. Koel, J. Vac. Sci. Technol. A 8 (1990) 2585.
[19] J.M. Gottfried, K.J. Schmidt, S.L.M. Schroeder, K. Christmann, Surf. Sci. 511 (2002) 65.
[20] Y. Xu, M. Mavrikakis, J. Phys. Chem. B 107 (2003) 9298.
[21] G. Mills, M.S. Gordon, H. Metiu, J. Chem. Phys. 118 (2003) 4198.
[22] H. Huber, D. McIntosh, G.A. Ozin, Inorg. Chem. 16 (1977) 975.
[23] H.S. Oh, J.H. Yang, C.K. Costello, Y.M. Wang, S.R. Bare, H.H. Kung, M.C. Kung, J. Catal. 210 (2002) 375.
[24] M.C. Payne, M.P. Teter, D.C. Allan, T.A. Arias, J.D. Joannopoulos, Rev. Mod. Phys. 64 (1992) 1045.
[25] B. Hammer, L.B. Hansen, J.K. Nørskov, Phys. Rev. B 59 (1999) 7413.
[26] S.A. Varganov, R.M. Olson, M.S. Gordon, J. Chem. Phys. 119 (2003) 2531.
[27] D. Vanderbilt, Phys. Rev. B 41 (1990) 7892.
[28] H. Grönbeck, P. Broqvist, J. Chem. Phys. 119 (2003) 3896.
[29] D.C. Liu, J. Nocedal, Math. Prog. 45 (1989) 503.
[30] I. Yudanov, G. Pacchioni, K. Neyman, N. Rösch, J. Phys. Chem. B 101 (1997) 2786.
[31] B. Hammer, Phys. Rev. Lett. 89 (2002) 16102.
[32] H. Grönbeck, P. Broqvist, J. Phys. Chem. B 107 (2003) 12239.
[33] C. Nordling, J. Österman, Physics Handbook, Studentlitteratur, Lund, Sweden, 1987.
[34] J.V. Barth, R.J. Behm, G. Ertl, Surf. Sci. 341 (1995) 62.
[35] S. Brazzelli, C. Di Valentin, G. Pacchioni, E. Giamello, M. Chiesa, J. Phys. Chem. B 107 (2003) 8498.
[36] J.D. Stiehl, T.S. Kim, S.M. McClure, C.B. Mullins, J. Am. Chem. Soc. 126 (2004) 1606.
[37] A. Eichler, J. Hafner, Phys. Rev. Lett. 79 (2003) 4481.
[38] B. Yoon, H. Häkkinen, U. Landman, J. Phys. Chem. A 107 (2003) 4066.
[39] G.J. Blyholder, J. Phys. Chem. 68 (1964) 2772.
[40] K. Hermann, P.S. Bagus, C.J. Nelin, Phys. Rev. B 35 (1987) 9467.
[41] P.S. Bagus, G. Pacchioni, Surf. Sci. 278 (1992) 427.
[42] B. Hammer, Y. Morikawa, J.K. Nørskov, Phys. Rev. Lett. 76 (1996) 2141.
[43] B. Hammer, O.H. Nielsen, J.K. Nørskov, Catal. Lett. 46 (1997) 31.